ACS NANO
Cite This: ACS Nano 2018, 12, 9521−9531
www.acsnano.org

ARTICLE

Ultrathin Gold Nanowires with the Polytetrahedral Structure of Bulk Manganese

Jorge A. Vargas,[†] Valeri Petkov,*[,†] El Said A. Nouh,[‡] Raj Kumar Ramamoorthy,[‡] Lise-Marie Lacroix,[‡] Romuald Poteau,[‡] Guillaume Viau,*[,‡] Pierre Lecante,[§] and Raul Arenal[⊥,#]

[†]Department of Physics, Central Michigan University, Mt. Pleasant, Michigan 48858, United States
[‡]Université de Toulouse, LPCNO, UMR 5215 INSA-CNRS-UPS, 135 Avenue de Rangueil, F-31077 Toulouse, France
[§]CEMES, France Centre d'Elaboration de Matériaux et d'Etudes Structurales, CEMES, CNRS, 29 Rue Jeanne Marvig, F-31055 Toulouse, France
[⊥]Laboratorio de Microscopias Avanzadas (LMA), Instituto de Nanociencia de Aragon (INA), U. Zaragoza, C/Mariano Esquillor s/n, 50018 Zaragoza, Spain
[#]ARAID Foundation, 50018 Zaragoza, Spain

Supporting Information

ABSTRACT: **Despite the intensive interest in thin gold nanowires for a variety of technologically important applications, key details of the mechanism of their formation and atomic-scale structure remain unknown. Here we synthesize highly uniform, very long, and ultrathin gold nanowires in a liquid-phase environment and study their nucleation and growth using *in situ* high-energy synchrotron X-ray diffraction. By controlling the type of solvents, reducing agents, and gold precursor concentration, it is shown that the nucleation and growth of gold nanowires involve the emergence and self-assembly of transient linear gold complexes, respectively. In sharp contrast with the face-centered-cubic bulk gold, the evolved nanowires are found to possess a tetrahedrally close packed structure incorporating distorted icosahedra and larger size coordination polyhedra of the type observed with the room-temperature phase of bulk manganese. We relate the complexes to synergistic effects between the selected precursor and reducing agents that become appreciable over a narrow range of their molar ratios. We attribute the unusual structural state of gold nanowires to geometrical frustration effects arising from the conflicting tendencies of assemblies of metal atoms to evolve toward attaining high atomic packing density while keeping the atomic-level stresses low, ultimately favoring the growth of cylindrical nanowires with a well-defined diameter and atomically smooth surface. Our work provides a roadmap for comprehensive characterization and, hence, better understanding of 1D metallic nanostructures with an unusual atomic arrangement and may have important implications for their synthesis and performance in practical applications.**

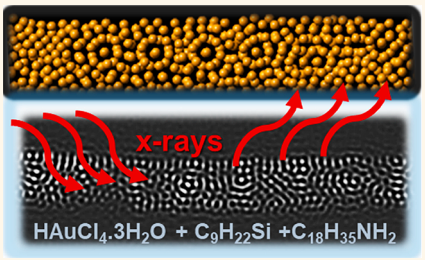

KEYWORDS: *1D nanomaterials, synthesis, liquid phase, Au nanowires, in situ synchrotron X-ray diffraction, 3D atomic structure*

Bulk gold (Au) has been used since ancient times in the production of jewelry, coins, and statues and as a decoration for buildings. Today, 1D Au nanostructures, in particular thin Au nanowires (NWs), attract a lot of interest because of their potential for applications in the fields of catalysis, molecular electronics, bioimaging, and drug delivery.[1−7] Au NWs have been produced by both top-down and bottom-up approaches, including electron beam irradiation of Au foils, vapor deposition, galvanic replacement reactions, soft-template-mediated growth in solution, and others. In addition, ordered arrays of Au NWs have been made in solution or deposited on surfaces aiming at developing devices with complex topology.[8−12] The structural and morphological characteristics of the NWs have been studied by small-angle X-ray scattering (SAXS), traditional X-ray diffraction (XRD), and, for the most part, high-resolution transmission electron microscopy (HR-TEM). However, thin metal NWs are prone to suffer significant structural defects and even break into pieces under the electron beam, rendering HR-TEM findings insufficient.[13] Besides, *in situ* HR-TEM studies on the nucleation and growth of Au NWs synthesized by bottom-up approaches are still difficult to perform. On a related frontier, theoretical studies have largely considered Au NWs as either pieces of a face-centered cubic (fcc) crystal or multishell structures of specific "magic" sizes.[14,15] While such considerations may be warranted for thick (many tens of nm) NWs and samples exposed to an intense electron beam, it is not

Received: July 3, 2018
Accepted: September 10, 2018
Published: September 10, 2018

DOI: 10.1021/acsnano.8b05036
ACS Nano 2018, 12, 9521−9531

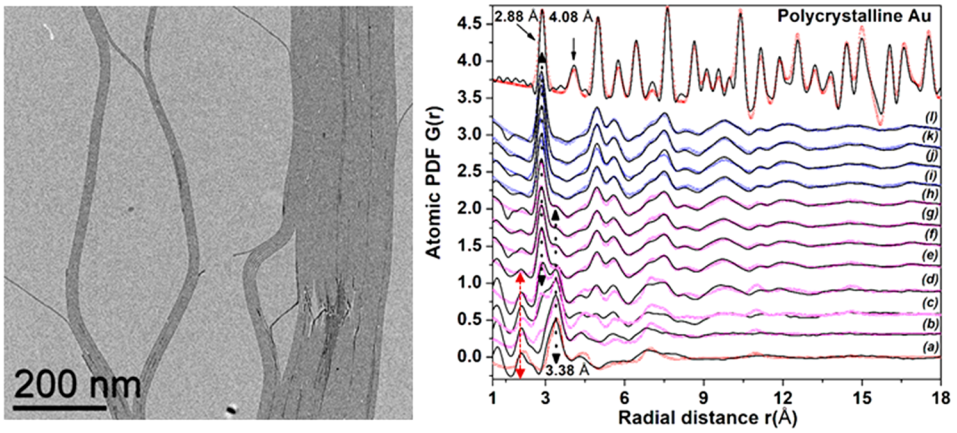

Figure 1. (Left) Representative TEM image of μm-long Au NWs obtained from a solution of $HAuCl_4{\cdot}3H_2O$, OY, and TIPS in hexane wherein the molar OY/Au and TIPS/OY ratios are 10 and 2.5, respectively. The NWs are highly uniform and have a diameter of about 2 nm. (Right) *In situ* atomic PDFs (black line) for (a) the fresh solution and the same solution aged for (b) 30 min, (c) 45 min, (d) 1 h, (e) 1.5 h, (f) 2 h, (g) 2.5 h, (h) 3 h, (i) 5 h, (j) 10 h, (k) 15 h, and (l) 20 h. The experimental PDF for the fresh solution is well approximated by a structure model (red line) featuring short chains of $\{Cl{-}Au^{I}{-}NH_2{-}R\}_n$ molecular complexes shown in Figure 7a. First-neighbor Au−Au pair distances/correlations in the chains appear as a relatively well-defined PDF peak positioned at about 3.38 Å. First-neighbor Au−organic species distances/correlations in the chains, where first-neighbor organic species are N and Cl, appear as a broad PDF peak centered at about 2.15 Å (red dotted arrow). The experimental PDFs for the solutions aged for less than 3 h are well approximated by a structure model (magenta line) featuring a mixture of short chains of Au atoms (Au−Au distance ~3.38 Å) and Au NWs (Au−Au distance ~2.86 Å). The NWs gradually grow both in size and in relative concentration with the time of aging at the expense of the chains (follow the evolution of atomic PDF data emphasized by black dotted arrows). The experimental PDFs for the solutions aged for more than 3 h are well approximated by a structure model (blue line) featuring Au NWs built from interconnected polyhedra with triangular vertices as shown in Figure 6(d). First-neighbor Au−Au pair distances in the NWs appear as a well-defined PDF peak centered at about 2.86 Å. The PDF for polycrystalline (bulk) Au standard (black line) is also shown for comparison. The PDF is reproduced very well by a model (red line) based on the fcc structure of bulk Au. First and second Au−Au pair distances in bulk Au appear as well-defined PDF peaks centered at about 2.88 and 4.08 Å, respectively (see solid black arrows). Note that the PDFs for NWs do not show a peak at 4.08 Å.

certain that detailed structure knowledge for thin Au NWs can be obtained by extrapolating results from casual studies. It is therefore imperative that a direct and noninvasive study on the nucleation and growth of Au NWs in a liquid-phase environment is conducted to achieve a good understanding of their nature and, hence, control over both their synthesis and functional properties.

Here we report results from a detailed study on the 3D structure of ultrathin and very long Au NWs as they are synthesized in a liquid-phase medium. The synthesis employs a well-established protocol based on first dissolving hydrogen tetrachloroaurate(III) trihydrate ($HAuCl_4{\cdot}3H_2O$) in hexane in the presence of oleylamine (OY) and then adding triisopropylsilane (TIPS) reductant to accelerate the reduction to $Au^{(0)}$. Prior studies have found that the concentration of OY strongly affects the type and morphology of the reaction product.[16] Hence, we studied $HAuCl_4{\cdot}3H_2O$ solutions in hexane, hereafter referred to as Au solutions for brevity, with different amounts of OY. For completeness, we also studied a Au solution in cyclohexane. More details of the synthesis protocol can be found in the Supporting Information (SI). Fresh solutions were immediately subjected to diffraction experiments using synchrotron X-rays with an energy of 58.62 keV (λ = 0.2115 Å). Data were taken in intervals of 5 min for up to 20 h in total. More details of the high-energy (HE)-XRD experiments can be found in the SI.

RESULTS AND DISCUSSION

Experimental *in situ* HE-XRD patterns for a fresh and aged Au solution in hexane wherein the molar OY/Au and TIPS/OY ratios are 10 and 2.5, respectively, are shown in Figure S1. As can be seen in the figure, the patterns are rather diffuse in nature, rendering traditional techniques for 3D structure studies of bulk metals difficult to apply to the nanosized Au samples studied here. Hence, the patterns were considered in terms of atomic pair distribution functions (PDFs) that have proven useful in structure studies on metallic particles suspended in liquids.[17] The PDFs are shown in Figure 1 (right). Details of the derivation of atomic PDFs from the HE-XRD patterns can be found in the SI. A representative TEM image of the product emerging from a (OY/Au = 10 and TIPS/OY = 2.5) solution of Au in hexane aged for 20 h is shown in Figure 1 (left). As can be seen in the image, the product is a strand of aligned, highly uniform, and μm-long Au NWs with a diameter of about 2 nm. Details of the TEM experiments can be found in the SI. Experimental *in situ* atomic PDFs for a (OY/Au = 10 and TIPS/OY = 2.5) solution of Au in hexane aged for a further 4 days are shown in Figure S2. The PDFs do not exhibit significant changes, remaining very similar to that for the (OY/Au = 10 and TIPS/OY = 2.5) solution of Au aged for only 20 h (compare with the PDF data set shown in Figure 1 (right). Experimental *in situ* HE-XRD patterns for a fresh and aged Au solution in hexane wherein the molar OY/Au and TIPS/OY ratios are 20 and 2.5, respectively, are shown in Figure S3. The respective atomic PDFs are shown in Figure S4 (right). Representative TEM image of the product emerging from a (OY/Au = 20 and TIPS/OY = 2.5) solution of Au aged for 20 h is shown in Figure S4 (left). As can be seen in the image, here the product is also a strand of aligned, highly uniform, and μm-long Au NWs with a diameter of about 2 nm. Experimental *in situ* atomic PDFs for a fresh and aged Au solution in cyclohexane wherein the molar OY/Au and TIPS/OY ratios are 10 and 2.5, respectively, are shown in Figure S5. The PDF for the product emerging from the (OY/Au = 10 and

DOI: 10.1021/acsnano.8b05036
ACS Nano 2018, 12, 9521−9531

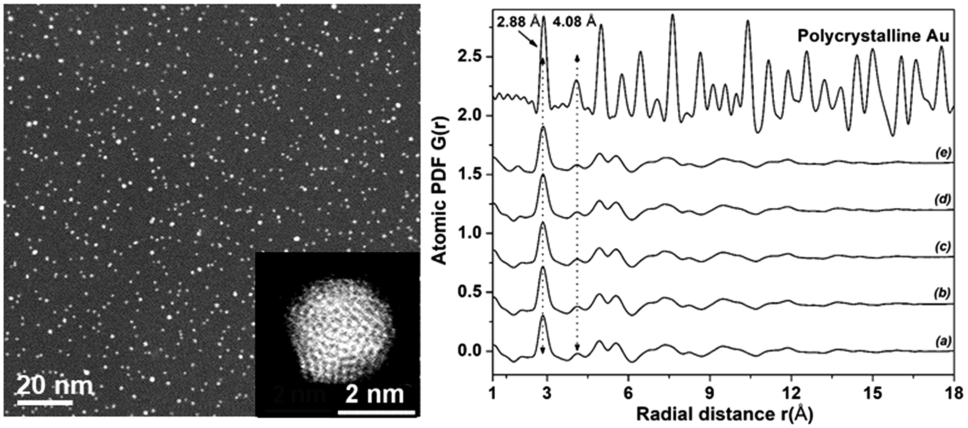

Figure 2. (Left) Representative HAADF-STEM images of monodispersed Au NPs obtained from a solution of $HAuCl_4 \cdot 3H_2O$, OY, and TIPS in hexane wherein the molar OY/Au and TIPS/OY ratios are 2.5 and 20, respectively. The NPs are shaped as polyhedra with round edges and have an average size of about 2 nm. (Right) *In situ* atomic PDFs for (a) the fresh solution and the same solution aged for (b) 1 h, (c) 2 h, (d) 3 h, and (e) 20 h. First- and second-neighbor Au−Au pair distances in the solutions appear as well-defined PDF peaks centered at about 2.86 and 4.08 Å (see the black dotted arrows), respectively. The PDFs are well approximated by a structure model featuring a distorted icosahedron (see Figures 4j and 6f). Note that correlations between Au and organic species in the solutions, where organic species are C, Cl, and N, do not appear in the PDFs for the solutions. The observation indicates that Au species in the solution have been reduced to metallic $Au^{(0)}$ atoms very fast (<5 min). The PDF for polycrystalline (bulk) Au standard is also shown for comparison. First and second Au−Au pair distances in bulk Au appear as well-defined PDF peaks centered at about 2.88 and 4.08 Å, respectively. The PDFs for the solution exhibit both peaks.

TIPS/OY = 2.5) solution of Au in cyclohexane aged for 20 h is virtually identical to those shown in Figures 1 (right), S2, and S4 (right). Evidently, Au NWs emerge from Au solutions in both hexane and cyclohexane wherein the molar OY/Au and TIPS/OY ratios are on the order of 10−20 and 2−3, respectively. Furthermore, the NWs remain stable in the mother liquor for days. Their stability has been shown to improve further by using phosphines as a capping agent.[18] As indicated by the respective PDF data sets in Figures 1 (right), S2, S4 (right), and S5, largely, Au NWs emerging from the variety of solutions studied here exhibit the same atomic-scale structure. The structure is not of an fcc type because the atomic PDFs for the NWs and bulk fcc Au shown in the figures disagree. In particular, Au NWs do not exhibit a second-neighbor Au−Au pair distance of 4.08 Å, which is characteristic of bulk Au and considered as its fcc-lattice parameter (see Figure S6). The NWs though exhibit a first-neighbor Au−Au pair distance of about 2.86 Å, which is very close to the Au−Au bonding distance in bulk Au (follow the black dotted arrows in Figures 1 (right), S4 (right), and S5). In line with the findings of independent X-ray photoelectron spectroscopy experiments, the observation indicates that Au atoms in the NWs are in a metallic (Au^0) state.[16]

Experimental *in situ* HE-XRD patterns for a fresh and aged Au solution in hexane wherein the molar OY/Au and TIPS/OY ratios are 2.5 and 20, respectively, are shown in Figure S7. Atomic PDFs derived from the patterns are shown in Figure 2 (right). Representative high-angle annular dark field scanning transmission electron microscopy (HAADF-STEM) images of the product emerging from a (OY/Au = 2.5 and TIPS/OY = 20) solution aged for 20 h are shown in Figure 2 (left). As can be seen in the images, this time the product is a collection of well-separated and monodisperse Au nanoparticles (NPs). The NPs appear as polyhedra with somewhat round edges and a diameter of about 2 nm. Experimental *in situ* atomic PDFs for a fresh and aged Au solution in hexane wherein the molar OY/Au and TIPS/OY ratios are 2 and 12.5, respectively, are shown in Figure S8. The PDFs are identical to those shown in Figure 2 (right). Experimental *in situ* atomic PDFs for a (OY/Au = 2 and TIPS/OY = 15) solution of Au in hexane aged for a further 4 days are shown in Figure S9. The PDFs do not exhibit significant changes, remaining identical to that for the (OY/Au = 2.5 and TIPS/OY = 20) solution of Au aged for 20 h (compare with the respective data set shown in Figure S8). Evidently, Au NPs emerge from Au solutions in hexane wherein the molar OY/Au and TIPS/OY ratios are $\leq$ 2.5 and $\geq$12.5, respectively, and, similarly to the case of Au NWs, remain stable in the mother liquor for days. Furthermore, as evidenced by the respective *in situ* atomic PDFs, the NPs are alike with respect to their atomic-level structure. The observation is in line with the results of independent TEM studies.[16] The structure bears some similarities to that of bulk fcc Au, but it is not quite the same (follow the dotted arrows and also compare the overall shape of the atomic PDFs for Au NPs and bulk Au shown in Figures 2 (right), S8, and S9).

To determine the atomic structure of Au NPs, the representative PDF data set shown in Figure 2 (right) was approached with several plausible models.[19,20] In line with the findings of HR-TEM and HAADF-STEM experiments, the models featured particles with a near-polyhedral shape and diameter of about 2 nm. Fcc-, hexagonal close-packed (hcp)-, body-centered cubic (bcc)-, icosahedral-, and decahedral-type model particles were considered. Fragments from complex crystal structures of metals, such as β-W- and α-Mn-type structures, were also considered. Note that β-W belongs to the so-called Frank−Kasper-type phases and α-Mn is closely related to them.[21,22] The models were optimized in terms of energy and equilibrated at room temperature by molecular dynamics (MD). Promising MD models were refined further against the experimental PDF data by reverse Monte Carlo (RMC) computations. Simultaneously, the model's energy was kept close to its minimal value obtained by MD. Details of the MD and RMC computations can be found in the SI. Representative modeling results are shown in Figure 3.

DOI: 10.1021/acsnano.8b05036
ACS Nano 2018, 12, 9521−9531

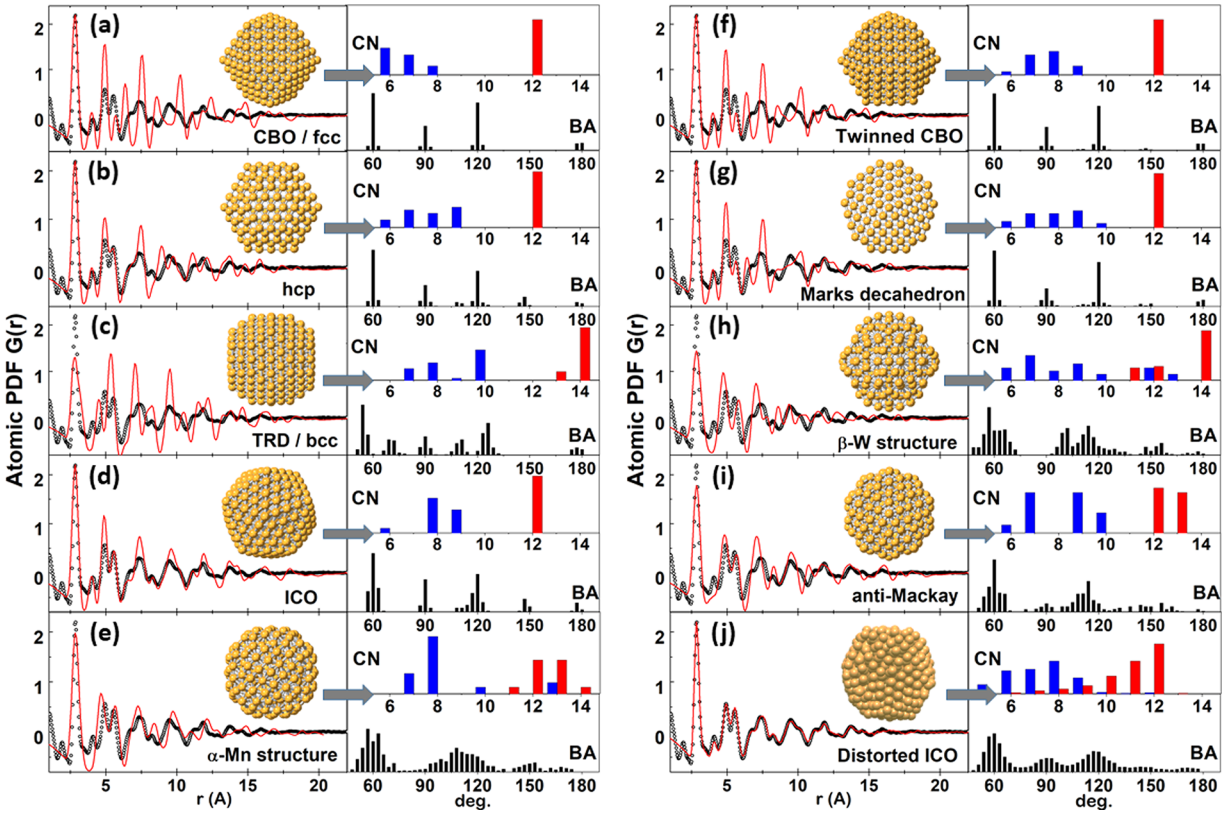

Figure 3. Comparison between the experimental (symbols) and computed (red line) PDFs for Au NPs. Computed PDFs are derived from structure models relaxed in terms of energy by MD and refined against the experimental PDF data by RMC as described in the text. The models feature (a) an fcc-type configuration with a cuboctahedral shape and (f) its twinned version, (b) an hcp-type configuration, (g) a configuration with the shape of the so-called Marks decahedron, (c) a bcc-type configuration with the shape of a truncated rhombic dodecahedron (TRD), fragments of the (h) *β*-W- and (e) *α*-Mn-type crystal structures, (i) a configuration with the shape of the so-called anti-Mackay polyhedron, (d) a configuration with an overall icosahedral symmetry and shape (ICO), and (j) its significantly distorted version. The configurations are shown as insets (circles in yellow). To emphasize their distinctiveness, the respective distribution of bond angles (BAs) (black bars) as well as surface (blue bars) and bulk (red bars) first coordination numbers (CNs) are also shown (follow the horizontal gray arrows). As can be seen in the figure, the levels of agreement with the experimental PDF data for the different model structures are significantly different. In particular, the goodness-of-RMC-fit indicator, R_w, for all but the structure model shown in (j) is above 20%. The value of R_w for the distorted ICO model is 9%.

Among all considered models, a 435-atom configuration featuring a considerably distorted icosahedron emerged as the most likely 3D structure of the Au NPs studied here. The configuration is shown in Figure 3j. The remarkable level of agreement between the configuration-derived and experimental PDF data is illustrated in Figure S10 in more detail. Despite that the distributions of bond angles (BAs) and first coordination numbers (CNs) in the configuration appear rather broad (see Figure 3j, right), the packing density of the configuration is almost as high (∼70%) as that (∼74%) of the fcc-type structure of bulk Au. This is one of the factors responsible for the observed similarity between the respective PDF data sets.

Likewise, the atomic structure of Au NWs was determined by approaching the representative experimental PDF data set shown in Figure 1(right) with several plausible models.[8,19,20,23] In line with the findings of HR-TEM experiments, the models featured atomic configurations with a near-cylindrical shape and diameter of about 2 nm. To account for the physical oscillations in the PDF data at higher r values (see Figures S12 and S13), the configurations had to be about 12 nm long. Wires running along the [111] and [110] directions of an fcc lattice, [001] direction of an hcp lattice, the so-called Boerdijk−Coxeter−Bernal (BCB) helix, spiral-type wires, and a wire built of attached Au NPs, *i.e.*, of attached icosahedra of the type shown in Figure 3j, were considered. Wire-type fragments of the *α*-Mn-, *β*-Mn-, *β*-W-, and Sm-type crystal structures were also considered. Note that *β*-Mn is a Frank−Kasper-type phase, while Sm exhibits a complex hcp-type structure with a multilayer (ABCB) stacking sequence. The sequence is related to the so-called 4H hexagonal phase. The phase has been observed with wire-, ribbon-, and planar-type Au nanostructures synthesized by the so-called crystal-phase controlled approach.[24−28] The models were optimized in terms of energy and equilibrated at room temperature by MD. With due care not to have their energy increased, promising MD models were refined further against the experimental PDF data by RMC. Representative modeling results are shown in Figures 4 and S11. As can be seen in the figures, an atomic configuration closely related to the room-temperature phase of manganese (*α*-Mn) appears fully consistent with the experimental data. The configuration is shown in Figure 4j and, in more detail, in Figure S12. The very good level of agreement between the configuration-derived and experimental PDF data is highlighted in Figures S12 and S13. Note that atoms in the *α*-Mn-type structure (≲70% packing efficiency)

DOI: 10.1021/acsnano.8b05036
ACS Nano 2018, 12, 9521−9531

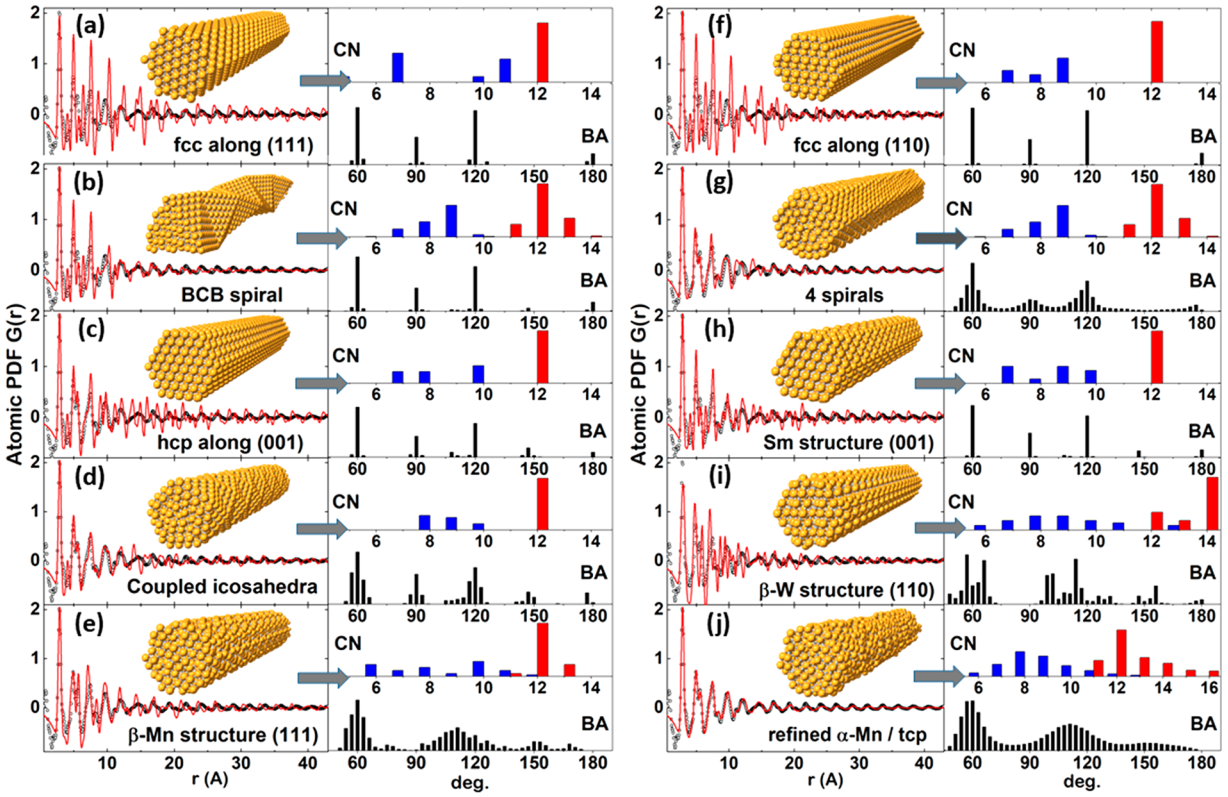

Figure 4. Comparison between the experimental (symbols) and computed (red line) PDFs for Au NWs. Computed PDFs are derived from structure models relaxed in terms of energy by MD and refined against the experimental PDF data by RMC as described in the text. The models feature wires running along (a) [111] and (f) [110] directions of an fcc lattice, (b) the so-called Boerdijk−Coxeter−Bernal (BCB) helix, (g) a spiral-type wire made of four coaxial layers, (c) a wire running along the [001] direction of an hcp lattice, wire-type fragments of the (i) *β*-W-, (e) *β*-Mn-, (h) Sm-, and (j) *α*-Mn-type crystal structures, and (d) a wire built of interconnected icosahedral Au NPs shown in Figure 3j (inset). Model wires are shown as insets (circles in yellow). To emphasize their distinctiveness, the respective distribution of bond angles (BAs) (black bars) as well as surface (blue bars) and bulk (red bars) first coordination numbers (CNs) are also shown (follow the horizontal gray arrows). As can be seen in the figure, the levels of agreement with the experimental PDF data for the different model structures are significantly different. In particular, the goodness-of-RMC-fit indicator, R_w, for all but the structure model shown in (j) is above 25%. The value of R_w for the *α*-Mn-type/tcp-type model is 11%.

are not as closely packed as atoms in the fcc-type structure (74% packing efficiency) of bulk Au are. In particular, atoms in the latter have a first CN of 12 and enclose both octahedral and tetrahedral interstices, whereas atoms in the former have a first CN of either 12, 13, or 16 and enclose tetrahedral interstices alone. Hence, the *α*-Mn-type structure is considered to be closely related to the so-called tetrahedrally, also known as a topologically, close-packed (tcp) structures, wherein polyhedra with a near-icosahedral symmetry (12 vertices) are combined with larger coordination polyhedra.[21,22] As indicated by the respective CNs and BAs shown in Figure 4j (right) and illustrated in Figure 6d, Au NWs can be well described as cylinders enclosing near-icosahedral polyhedra interfaced with a relatively small number of larger polyhedra, including the so-called Friauf polyhedra with 16 vertices. The small number of the latter does not indicate a significant departure from the tcp-type structures. Merely, it reflects the fact that, contrary to bulk tcp phases, ultrathin Au NWs possess a very large fraction (~43%) of undercoordinated surface atoms per unit volume.

To validate the findings of the PDF analysis of the *in situ* HE-XRD data, we carried out *ex situ* HAADF-STEM experiments on Au NWs aged for less than 24 h. To avoid changes in their structure, the NWs were exposed to a low-intensity electron beam for a very short period of time.[29,30] Representative HAADF-STEM images of Au NWs are shown in Figures 5a, 6a, and S14a−d. The images confirm that Au NWs studied here are not stacks of near-parallel atomic layers arranged in an fcc-type sequence observed with Au NWs studied by others.[11,31] The NWs do not appear as near-regular BCB helixes either.[32] Some surface atomic configurations in the Au NWs though exhibit 5-fold rotational symmetry seen with about 50 nm long and rather uneven binary Ag_3Au_1 alloy NWs.[23] The latter have been recognized as either entangled BCB helices or helical arrays of decahedra. Both structures are inconsistent with the *μ*m-long and much more uniform monometallic Au NWs studied here (*e.g.*, compare images in Figure S14 here with images in Figure 3 in ref 23). A representative fragment of the NWs, as revealed by HAADF-STEM, and a surface fragment of their tcp-type model structure, as determined by PDF analysis of *in situ* HE-XRD data, are compared side by side in Figure 6b,c. The resemblance between the two is astounding. An HAADF-STEM image of Au NPs and a 2D projection of their 435-atom model structure are shown in Figure 6e and f, respectively. The two resemble each other to a very high degree. Certainly, data in Figure 6a−f attest to the reliability of the structure studies conducted here.

Several mechanisms for the nucleation and growth of ultrathin and *μ*m-long Au NWs in a liquid-phase environment have been proposed, including a preferential adsorption of

DOI: 10.1021/acsnano.8b05036
ACS Nano 2018, 12, 9521−9531

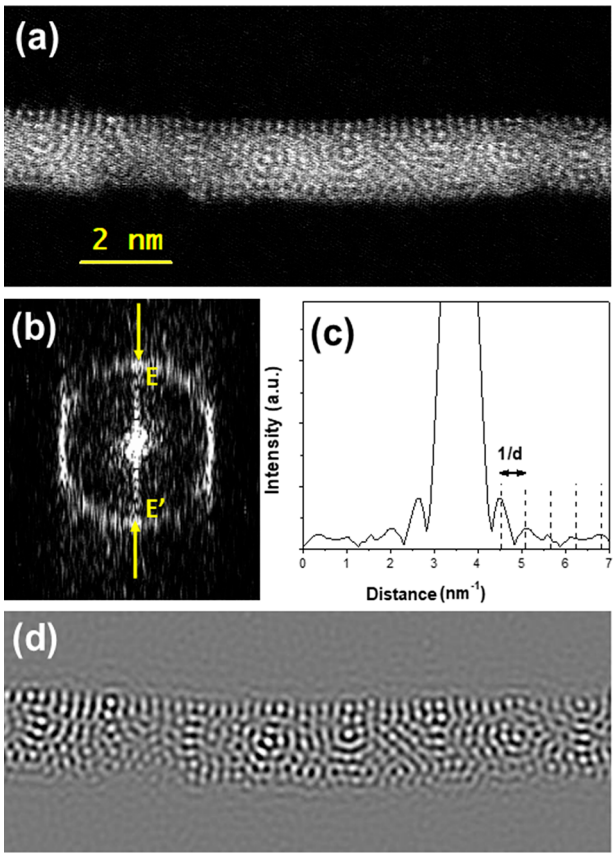

Figure 5. (a) Representative HAADF-STEM image of a segment of Au NW and (b) its Fourier transform. The transform can be considered as an electron diffraction pattern of the NW. (c) Intensity profile along the equatorial line (EE′) of the Fourier transform. The uniform diameter of Au NWs, *d*, is attested by the oscillatory behavior of the (EE′) line, where the period of the oscillations is 1/*d*. Notably, a similar pattern has been observed with single- and double-wall carbon nanotubes, which are known to exhibit a very uniform thickness.[33,34] (d) Fourier-filtered rendition of the image in (a). Note that the image was acquired over a very short exposure time (<1 s) because, as once again demonstrated in Figure S16, Au NWs are unstable when exposed to an intense electron beam.

surfactants on particular facets of fcc-type Au seeds, an oriented attachment of icosahedral or other type polyhedral Au NPs, micelle-template-assisted growth of 1D fcc Au nanostructures, and others.[16,35−37] The α-Mn-type structure and atomically smooth surface of Au NWs studied here rule out these mechanisms. Hence, we considered others, in particular the emergence of transient molecular complexes that would assist the growth of uniform 1D tcp-type Au nanostructures. The presence of such complexes was hinted by the peculiar time evolution of the low-*r* peaks in the *in situ* PDFs for Au NWs shown in Figures 1(right), S4, and S5. DFT calculations indicated that near-straight chains of $\{Cl{-}Au^{I}{-}NH_2{-}R\}_n$ molecular units (R = C_3H_7), shown in Figure 7a, could be the backbone of transient $\{Cl{-}Au^{I}{-}NH_2{-}OY\}$ complexes (OY = $C_{18}H_{35}$) assisting the growth of highly uniform, very long, and ultrathin Au NWs seen in Figure 1 (left). The calculations are described in the SI and, in more detail, in ref 38. The DFT result is not a surprise because, due to aurophilic interactions and hydrogen bonding, molecular $Au^{(I)}$ units tend to "polymerize" in linear complexes.[39] In general, the term aurophilic interactions is used to describe the affinity between two closed-shell $Au^{(I)}$ species (with the valence electronic configuration $5d^{10}$) driven by relativistic effects and the high electronegativity of gold. Notably, due to this affinity, linear $\{Cl{-}Au^{I}{-}NH_2{-}OY\}$ molecular complexes in solution may be literally drawn to each other, forming polynuclear complexes involving nearby mixed-valence $Au^{I}(5d^{10})/Au^{0}(5d^{10}6s^{1})$ and/or metallic $Au^{(0)}$ species.[39] A tentative balanced chemical reaction for the complexation of $HAuCl_4{\cdot}3H_2O$ by OY, reduction of the resulting $Au^{(III)}$ complexes into $Au^{(I)}$ complexes, formation of chains of $\{Cl{-}Au^{I}{-}NH_2{-}R\}$ units, and reduction by TIPS of the chains into metallic $Au^{(0)}$ species is given in the SI (see Scheme 1). An assembly of such linear complexes indeed approximates very well the *in situ* PDF data for Au solutions aged for a short period of time, *e.g.*, aged for up to 1.5 h for the Au solution producing the PDF data shown in Figure 1 (right) and up to about 3 h for the Au solution producing the PDF data shown in Figure S4 (right). In particular, under the NW growth conditions, the average $Au^{(I)}{-}Au^{(I)}$ distances in the linear complexes/chains appear as a well-defined PDF peak centered at about 3.4−3.5 Å. Furthermore, the average $Au^{(I)}$−nearby organic species distances in the chains, where nearby organic species are N and Cl, appear as a well-defined PDF peak centered at about 2.15−2.35 Å. The peaks gradually disappear with the progressing NW growth, and a well-defined $Au^{(0)}{-}Au^{(0)}$ bonding distance appears instead (follow the vertical dotted lines in Figures 1 (right), S4, and S5). This is the first experimental evidence that chain-type $\{Cl{-}Au^{I}{-}NH_2{-}R\}_n$ complexes involving aurophilic bonds, soluble in (cyclo)hexane, can form, assist the growth of ultrathin Au NWs, and gradually disappear in the process. A likely mechanism for the structural evolution of Au NWs studied here is sketched in Figure 7. Here it is to be noted that Au−Au distances significantly longer than the bulk value of 2.88 Å have been considered in structure studies of suspended metallic Au chains.[40,41]

Oleylamine is a multifunctional reagent for the production of nanosized metallic materials because it can serve as both a surfactant and reducing agent. It is considered that in the presence of stronger reductants, such as TIPS, the role of OY is largely reduced to a ligand for $Au^{(I)}$ precursors and surfactant for $Au^{(0)}$ nanostructures. Not surprisingly, results from the present study indicate that when the percentage of OY in the solution of $HAuCl_4{\cdot}3H_2O$ and TIPS in (cyclo)hexane is low, *e.g.*, for molar OY/Au and TIPS/OY ratios of $\leq$2.5 and $\geq$12.5, respectively, $Au^{(I)}$ species in the solution are directly reduced to metallic $Au^{(0)}$ species. Moreover, the latter near instantly assemble in Au NPs (see the lack of time evolution of the *in situ* PDFs shown in Figures 2, right, S8, and S9) with an overall icosahedral symmetry (see modeling results summarized in Figure 3) and diameter of about 2 nm (see HAADF-STEM images in Figure 2, left). The largely isotropic character of metallic bonding, favoring the formation of nanostructures with the highest possible atomic packing density, may explain the preference for polyicosahedral structure in the NPs over the possible fcc-type structure. Small-size icosahedra (*e.g.*, the icosahedron shown in Figure 3d) have higher atomic packing density and so higher stability, *i.e.*, lower energy, in comparison to atomic configurations with an overall fcc-type symmetry (*e.g.*, the cuboctahedron shown in Figure 3a).[21,22,42] The exclusively triangular faces of the instantly formed icosahedral Au NPs though have to stretch in order for the NPs to continue growing in a space-filling structure. Additionally, the

DOI: 10.1021/acsnano.8b05036
ACS Nano 2018, 12, 9521−9531

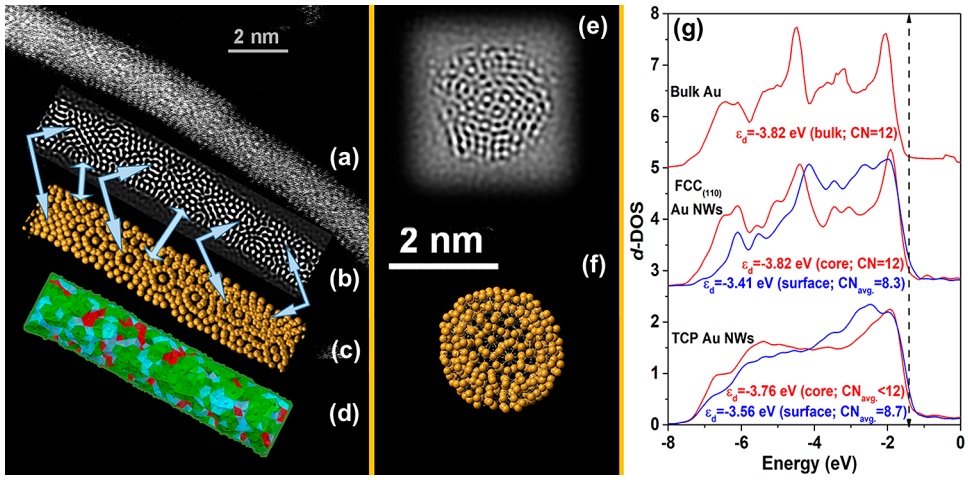

Figure 6. (a) Representative HAADF-STEM image of a segment of Au NW and (b) a Fourier filtered rendition of it. (c) Segment of the 3D model of Au NWs shown in Figure 4j (top two surface layers shown). Arrows point to atomic configurations characteristic of the surface of Au NWs as revealed by the independent HAADF-STEM experiments and structure modeling guided by *in situ* HE-XRD/PDF data. The configurations are markedly similar. (d) Polyhedral representation of the refined 3D model of Au NWs partitioned into (green) icosahedral, (blue) 13−14-vertex and (red) 15−16-vertex polyhedral units. The units have only triangular faces and so a rounded shape, thus forming a cylinder-type NW with an atomically smooth surface. (e) Representative HAADF-STEM image of Au NPs showing an atomic contrast consistent with icosahedral symmetry. (f) Projection of the 3D model of Au NPs derived from *in situ* HE-XRD/PDF data. The atomic configurations shown in (e) and (f) closely resemble each other. (g) Calculated d-DOS for atoms inside (red line) and at the surface (blue line) of bulk fcc Au, $fcc_{(110)}$ Au NWs, and tcp Au NWs. The d-DOS for the NWs are calculated from slices of the respective model structures shown in Figure 4. The structures/slices have the same surface to unit volume ratio of about 43%. The average energy of the d electrons (or d-band center), ϵ_d, of surface and core atoms, and their average CNs, are given for each data set in the respective color. The Fermi energy is set to 0 eV for clarity. Vertical broken line is an aid to the eye.

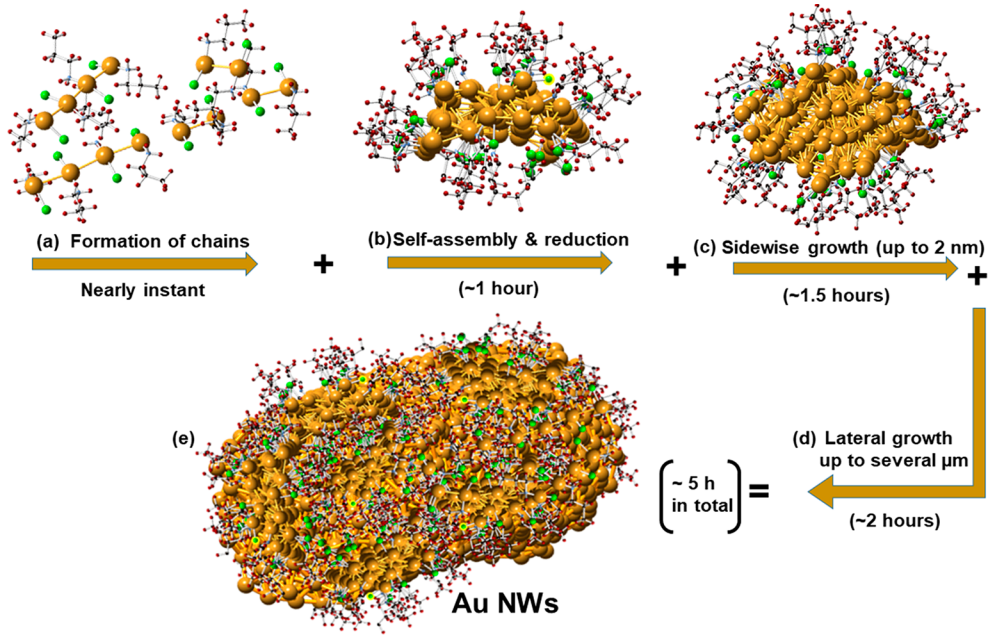

Figure 7. Schematic illustration of the formation of Au NWs in a solution of $HAuCl_4 \cdot 3H_2O$, OY, and TIPS in hexane wherein the molar OY/Au and TIPS/OY ratios are 10 and 2.5, respectively. For reference, this is the case of Au NWs shown in Figure 1, left. (a) Short chains of $\{Cl-Au^{I}-NH_2-R\}_n$ molecular units are formed in the solution and, due to intrachain aurophilic interactions and likely excluded volume effects, (b) self-assemble/aggregate, thus giving rise to (c) clusters of densely packed Au atoms with a diameter of about 2 nm. (d) The accumulating high tensile strain in the clusters precludes their further growth in 3D as multishell icosahedra. (e) The clusters though are free to relax and grow in 1D until all molecular complexes in the solution are consumed. To maintain the density of the atomic packing high and withstand the concomitant atomic-level stresses, the NWs adopt a tcp-type structure (see Figures 4j and 6d). Hence, their surface remains smooth at the atomic level (see Figures 5a and 6a). Au atoms are in yellow, Cl atoms are in green, N atoms are in gray, and H atoms are in red.

density of icosahedral packing of equal-size atoms is known to diminish gradually to about 70% as the number of shells in the icosahedron increases to about 5, that is, when its size exceeds 2 nm.[42] Both the decreased packing density and increased

DOI: 10.1021/acsnano.8b05036
ACS Nano 2018, 12, 9521−9531

tensile stress would preclude the growth of Au NPs beyond 2 nm in 3D, and so they are likely to end up as imperfect icosahedra, as observed here.

When the percentage of oleylamine in the solution is somewhat higher, *e.g.*, for molar OY/Au and TIPS/OY ratios of approximately 10−20 and 2−3, respectively, chain-type $\{Cl-Au^{I}-NH_2-R\}_n$ complexes emerge due to specific interactions between the Au precursor ($HAuCl_4{\cdot}3H_2O$), OY, and TIPS. Notably, due to their rod-like shape and mutual attraction arising from interchain aurophilic interactions, the complexes would tend to align and assemble side-by-side, thus forming Au nanostructures with a cylindrical shape. Excluded volume effects may also contribute to the process.[43] Concurrently, the reduced Au^0 atoms in the nanostructures would tend to pack with high efficiency, *e.g.*, by mainly arranging in an icosahedral manner. As discussed above, the radial growth of monometallic icosahedra is increasingly impeded by the simultaneously increasing atomic-level stresses, and so their diameter is limited to about 2 nm. Given the presence of linear$\{Cl-Au^{I}-NH_2-R\}_n$ complexes in the solution though, each of the cylinder-like Au nanostructures may keep evolving in 1D. As the results of our structure study show, the conflicting tendencies of evolving Au "nanocylinders" to attain high atomic packing density and simultaneously maintain the level of tensile stresses low are reconciled by the constituent Au atoms arranging in a tetrahedrally close packed structure. The structure consists of icosahedra and larger size polyhedra alternating in a 1D sequence, as shown in Figure 6d. The former provide high atomic packing density, and the latter relax the generated icosahedral strain. Because both the icosahedra and larger size polyhedra have only triangular faces and a near-spherical shape, the evolved "nanocylinders" are likely to appear with an atomically smooth surface and, hence, reduced surface energy. Oleylamine surfactants adsorbed on the surface of the "nanocylinders" may also contribute to the minimization of their surface energy.[16] This explains why Au NWs studied here appear as smooth cylinders and not as sausages made of icosahedral Au NPs.

When the percentage of oleylamine in the solution is increased further, *e.g.*, when the molar OY/Au and TIPS/OY become ≥20 and ≤2.5, respectively, the specific interactions, *i.e.* synergism, between the Au precursor, OY, and TIPS leading to the formation of individual$\{Cl-Au^{I}-NH_2-R\}_n$ complexes largely disappears. A lamellar phase of composition $[Cl-Au^{I}-OY]$ precipitates instead.[18,35,38] The reduction of $Au^{(I)}$ species in the lamellar phase is extremely slow, if any, and so the yield of Au NWs becomes very low. Apparently, two major factors control the synthesis of highly uniform, very long, and ultrathin Au NWs in a liquid-phase environment, *e.g.*, by dissolving a Au precursor, such as $HAuCl_4{\cdot}3H_2O$, and reductants, such as OY and TIPS, in nonpolar solvents, such as (cyclo)hexane. The first factor is the presence of synergistic effects between the precursor and reducing agents, leading to the emergence of transient chain-like $Au^{(I)}$ complexes that, due to interchain aurophilic interactions and likely excluded volume effects, can self-assemble into nanostructures with a cylindrical shape.[39,43,44] Monovalent $Au^{(I)}$ species inside the nanostructures are reduced to metallic $Au^{(0)}$ species. Atoms at the surface of the nanostructures are in a mixed $Au^{I}(5d^{10})/Au^{0}(5d^{10}6s^{1})$ valence state and likely coordinated by oleylammonium chloride and/or oleylamine ligands.[16] The second factor is the competition between the natural tendencies of $Au^{(0)}$ species in the emerging nanostructures to pack with high efficiently and, at the same time, inch toward a low strain energy state. The competition is causing $Au^{(0)}$ species to cohere in a tcp-type manner, thereby allowing the nanostructures to evolve in 1D as uniform (*i.e.*, free from staking faults, twin defects, and others of the type) cylinders with an atomically smooth (*i.e.*, lacking well-expressed facets, edges, and corners) surface. The evolved tcp Au NWs are stable in the mother liquor and can even be organized in periodic superlattices. Furthermore, the parameters of these superlattices can be tuned by using different surface ligands.[18] Altogether, the NWs appear to be an unusual phase of Au that can be produced at room temperature by a liquid-phase synthesis involving certain types of solvents, reducing agents, gold precursor, and surfactant intermixed in adequate proportions. Under the particular thermodynamic conditions and environment, the phase lowers its free energy, *i.e.*, increases its stability, by adopting a tcp-type structure. The phase though is metastable in a sense that, when taken out of its natural environment and heated, *e.g.*, when exposed to an intense electron beam under vacuum, it undergoes an irreversible structural phase transition into fcc Au, including disintegrating into pieces (see Figure S16). As briefly discussed below, this would not preclude its potential use in practical applications at near-ambient conditions.

DFT calculations, described in the SI, show that the electronic structure of tcp Au NWs, in particular the valence d-electron density of states (d-DOS) and its average energy position (ϵ_d), changes beyond the usual finite size effects observed with nanostructured fcc Au. In particular, as can be seen in Figure 6g, the reduced dimensionality of $fcc_{(110)}$ Au NWs affects mostly the d-DOS and ϵ_d for atoms at their surface, which are either seven-, eight-, or nine-fold coordinated. The bulk d-DOS for the NWs remains largely unaffected, *i.e.*, nearly identical to that of bulk fcc Au. That is because atoms inside both structures are densely packed in an fcc-type manner and so have the usual CN of 12. On the other hand, the reduced dimensionality, smooth cylindrical surface, and unusual structure of tcp Au NWs affect the d-DOS and ϵ_d for both atoms at their surface and atoms in their interior. Furthermore, due to the broad distribution of surface CNs (compare data in Figure 4f and j), changes in the surface d-DOS and ϵ_d for tcp Au NWs appear different from those found with $fcc_{(110)}$ Au NWs. Thus, the physicochemical properties of tcp Au NWs, including surface reactivity, may be expected to differ from those exhibited by fcc-type Au NWs.[1,45] Nearby surface sites on smooth tcp Au NWs are more likely to exhibit significantly different coordination and so affect each other's reactivity such that the usual relationship between the binding energy of reactants and reaction intermediates on fcc Au surfaces changes in a way that increases the kinetics of particular chemical reactions.[46] Indeed, given their unusual morphology and electronic structure, tcp Au NWs are likely to find use in applications beyond the current expectations.

CONCLUSIONS

Tetrahedrally close-packed structures are observed in materials ranging from simple metals (Mn) and alloys (Frank−Kasper phases) to self-assembled nanoparticles and diblock copolymers.[21,22,47,48] It is believed that the structures are formed when the arrangement of atoms in space is frustrated by strongly competing tendencies. In the case of the room-temperature phase of Mn, α-Mn, the tendencies are the drive

DOI: 10.1021/acsnano.8b05036
ACS Nano 2018, 12, 9521−9531

to maximize the bond strength and, according to Hund's rule, achieve a high magnetic spin moment.[49] As the results of the present study show, when brought together in a 1D nanostructure by self-assembly of linear complexes dispersed in an isotropic solution, Au($5d^{10}6s^1$) atoms respond to the usual drives to pack with high efficiency and yet avoid highly packed but strained configurations, such as multishell icosahedra, in a similar manner, that is, arrange in a tcp structure of the type adopted by Mn($3d^5 4s^2$) atoms. Given the communality between the two cases and plethora of tcp alloys between metals with different elemental size and electronic structure, often prepared by unconventional techniques, the creation of 1D metallic nanostructures with an unusual atomic arrangement *via* liquid-phase synthesis appears a wide-open avenue for further investigations and practical applications.

METHODS

Sample Preparation. Nanosized gold samples were prepared at room temperature by dissolving hydrogen tetrachloroaurate(III) trihydrate ($HAuCl_4 \cdot 3H_2O$) in hexane (C_6H_{14}) in the presence of oleylamine ($C_{18}H_{35}NH_2$) and then adding triisopropylsilane ($C_9H_{22}Si$) reductant to accelerate the reaction.[16,18] The solution was aged at room temperature without stirring. Several batches of samples were prepared varying the concentrations as detailed in the SI.

TEM and HAADF-STEM. TEM measurements were done on a JEOL JEM 1400 microscope. Exemplary TEM images are shown in Figures 1 (left) and S4 (left). HAADF measurements coupled with STEM were done on a TEM FEI Titan low-base 60-300 microscope. Exemplary HAADF-STEM images are shown in Figures 2 (left), 5a, 6a, S14, and S16. More details of the TEM and HAADF-STEM experiments can be found in the SI.

***In Situ* High-Energy X-ray Diffraction.** These experiments were carried out at the beamline 11-ID-B at the Advanced Photon Source, Argonne, using X-rays with an energy of 58.62 keV (λ = 0.2115 Å). HE-XRD data were taken in intervals of 5 min for 1 min each. In total, 210 patterns for each of the samples were obtained over 20 h of data collection time. The patterns covered wave vectors in the range of 1 to 25 $Å^{-1}$ with a q-space resolution proven acceptable for atomic pair distribution function studies on metallic NPs in solution.[17,50] Atomic PDFs derived from the HE-XRD patterns in Figures S1, S3, and S7 are shown in Figures 1 (right), S4 (right) and 2 (right), respectively. More details of the HE-XRD experiments can be found in the SI.

Atomic Structure Modeling. For both Au NPs and NWs, several structure models were generated and optimized in terms of energy by classical MD. Best MD models were refined against the experimental atomic PDFs by RMC.[51] The refinement was necessary because actual metallic NPs and NWs exhibit significant atomic relaxation, in particular close to their surface, which may not be captured by MD alone, *i.e.*, without experimental input. Details of MD and RMC computations can be found in the SI.

Electronic Structure Calculations. The electronic structure of Au NWs, in particular the d-band-projected density of states, was computed by DFT using the Vienna Ab-initio Simulation Package (VASP).[52] Details of the calculations can be found in the SI.

ASSOCIATED CONTENT

Supporting Information

The Supporting Information is available free of charge on the ACS Publications website at DOI: 10.1021/acsnano.8b05036.

Additional details for synthesis, HE-XRD experiments, and DFT calculations (PDF)

3D structure modeling (AVI)

AUTHOR INFORMATION

Corresponding Authors

*E-mail: petko1vg@cmich.edu.

*E-mail: gviau@insa-toulouse.fr.

ORCID

Valeri Petkov: 0000-0002-6392-7589

Romuald Poteau: 0000-0003-4338-174X

Guillaume Viau: 0000-0001-7062-4183

Raul Arenal: 0000-0002-2071-9093

Notes

The authors declare no competing financial interest.

ACKNOWLEDGMENTS

This work was supported by DOE-BES grant DE-SC0006877. The authors acknowledge financial support from the Labex NEXT, No. 11 LABX 075, and the European Associated Laboratory LEA TALEM. E.S.A.N. thanks the French Institute in Cairo (Egypt), the Science and Technology Fund (STDF), and INSA Toulouse for awarding a Fellowship to support this research. E.S.A.N. gratefully acknowledges the help from Egyptian Nuclear Materials Authority (Cairo) for granting him a sabbatical leave to carry out this work at INSA. This work used resources of the Advanced Photon Source at the Argonne National Laboratory provided by the DOE Office of Science under contract no. DE-AC02-06CH11357. Thanks are due to Dr. K. Beyer for the help with the HE-XRD experiments. The HR-STEM studies were conducted at the Laboratorio de Microscopias Avanzadas, Instituto de Nanociencia de Aragon, Universidad de Zaragoza, Spain. R.A. gratefully acknowledges the support from the Spanish Ministry of Economy and Competitiveness (MINECO) through grant MAT2016-79776-P (AEI/FEDER, UE). R.P. thanks the HPCs CALcul en MIdi-Pyrénées (CALMIP-EOS, grant P0611) and the Grand Equipement National de Calcul Intensif (GENCI-TGCC, grant 0810168) for generous allocations of computer time.

REFERENCES

(1) Zhu, W.; Zhang, Y. J.; Zhang, H.; Lv, H.; Li, Q.; Michalsky, R.; Peterson, A. A.; Sun, S. Active and Selective Conversion of CO_2 to CO on Ultrathin Au Nanowires. *J. Am. Chem. Soc.* **2014**, *136*, 16132−16135.

(2) Wang, C.; Hu, Y.; Lieber, C. M.; Sun, S. Ultrathin Au Nanowires and Their Transport Properties. *J. Am. Chem. Soc.* **2008**, *130*, 8902−8903.

(3) Gong, S.; Schwalb, W.; Wang, Y.; Chen, Y.; Tang, Y.; Si, J.; Shirinzadeh, B.; Cheng, W. A Wearable and Highly Sensitive Pressure Sensor with Ultrathin Gold Nanowires. *Nat. Commun.* **2014**, *5*, 3132.

(4) Maurer, J. H. M.; González-García, L.; Reiser, B.; Kanelidis, I.; Kraus, T. Templated Self-Assembly of Ultrathin Gold Nanowires by Nanoimprinting for Transparent Flexible Electronics. *Nano Lett.* **2016**, *16*, 2921−2925.

(5) Kuo, C.-W.; Lai, J.-J.; Wei, K. H.; Chen, P. Surface Modified Gold Nanowires for Mammalian Cell Transfection. *Nanotechnology* **2018**, *19*, 025103.

(6) Yoo, S. M.; Kang, M.; Kang, T.; Kim, D. M.; Lee, S. Y.; Kim, B. Electrotriggered, Spatioselective, Quantitative Gene Delivery into a Single Cell Nucleus by Au Nanowire Nanoinjector. *Nano Lett.* **2013**, *13*, 2431−2435.

(7) Cross, C. E.; Hemminger, J. C.; Penner, R. M. Physical Vapor Deposition of One-Dimensional Nanoparticle Arrays on Graphite: Seeding the Electrodeposition of Gold Nanowires. *Langmuir* **2007**, *23*, 10372−10379.

DOI: 10.1021/acsnano.8b05036
ACS Nano 2018, 12, 9521−9531

(8) Kondo, Y.; Takayanagi, K. Synthesis and Characterization of Helical Multi-Shell Gold Nanowires. *Science* **2000**, *289*, 606−608.
(9) Huo, Z.; Tsung, C.-K.; Huang, W.; Zhang, X.; Yang, P. Sub-Two Nanometer Single Crystal Au Nanowires. *Nano Lett.* **2008**, *8*, 2041−2044.
(10) Lu, X.; Yavuz, M. S.; Tuan, H.-Y.; Korgel, B. A.; Xia, Y. Ultrathin Gold Nanowires Can. Be Obtained by Reducing Polymeric Strands of Oleylamine−AuCl Complexes Formed *via* Aurophilic Interaction. *J. Am. Chem. Soc.* **2008**, *130*, 8900−8901.
(11) Yu, Y.; Cui, F.; Sun, J.; Yang, P. Atomic Structure of Ultrathin Gold Nanowires. *Nano Lett.* **2016**, *16*, 3078−3084.
(12) Bai, H.; Xu, K.; Xu, Y.; Matsui, H. Fabrication of Au Nanowires of Uniform Length and Diameter using a Monodisperse and Rigid Biomolecular Template: Collagen-Like Triple Helix. *Angew. Chem., Int. Ed.* **2007**, *46*, 3319−3322.
(13) Lacroix, L.-M.; Arenal, R.; Viau, G. Dynamic HAADF-STEM Observation of a Single-Atom Chain as the Transient State of Gold Ultrathin Nanowire Breakdown. *J. Am. Chem. Soc.* **2014**, *136*, 13075−13077.
(14) Iacovella, C.; French, W. R.; Cook, B. G.; Kent, P. R. C.; Cummings, P. T. Role of Polytetrahedral Structures in the Elongation and Rupture of Gold Nanowires. *ACS Nano* **2011**, *5*, 10065−10073.
(15) Tossati, E.; Prestipino, S. Weird Gold Nanowires. *Science* **2000**, *289*, 561−563.
(16) Loubat, A.; Impéror-Clerc, M.; Pansu, B.; Meneau, F.; Raquet, B.; Viau, G.; Lacroix, L.-M. Growth and Self-Assembly of Ultrathin Au Nanowires into Expanded Hexagonal Superlattice Studied by *in Situ* SAXS. *Langmuir* **2014**, *30*, 4005−4012.
(17) Petkov, V.; Peng, Y.; Williams, G.; Huang, B.; Tomalia, D.; Ren, Y. Structure of Gold Nanoparticles Suspended in Water Studied by X-ray Diffraction and Computer Simulations. *Phys. Rev. B: Condens. Matter Mater. Phys.* **2005**, *72*, 195402.
(18) Nouh, E. S. A.; Baquero, E. A.; Lacroix, L.-M.; Delpech, F.; Poteau, R.; Viau, G. Surface-Engineering of Ultrathin Gold Nanowires: Tailored Self-Assembly and Enhanced Stability. *Langmuir* **2017**, *33*, 5456−5463.
(19) Marks, L. D. Experimental Studies of Small Particle Structures. *Rep. Prog. Phys.* **1994**, *57*, 603−649.
(20) Ferrando, R.; Jellinek, J.; Johnston, R. L. Nanoalloys: From Theory to Applications of Alloy Clusters and Nanoparticles. *Chem. Rev.* **2008**, *108*, 845−910.
(21) Frank, F. C.; Kasper, J. S. Complex Alloy Structures Regarded as Sphere Packings. I. Definitions and basic principles. *Acta Crystallogr.* **1958**, *11*, 184−190.
(22) Frank, F. C.; Kasper, J. S. Complex Alloy Structures Regarded as Sphere Packings. II. Analysis and Classification of Representative Structures. *Acta Crystallogr.* **1959**, *12*, 483−499.
(23) Velazquez-Salazar, J. J.; Esparza, R.; Mejía-Rosales, S. J.; Estrada-Salas, R.; Ponce, A.; Deepak, F. L.; Castro-Guerrero, C.; José-Yacamán, M. Experimental Evidence of Icosahedral and Decahedral Packing in One-Dimensional Nanostructures. *ACS Nano* **2011**, *8*, 6272−6278.
(24) Huang, X.; Li, S.; Huang, Y.; Wu, S.; Zhou, X.; Li, S.; Gan, C. L.; Boey, F.; Mirkin, C. A.; Zhang, H. Synthesis of Hexagonal Close-Packed Gold Nanostructures. *Nat. Commun.* **2011**, *2*, 292.
(25) Fan, Z.; Bosman, M.; Huang, X.; Huang, D.; Yu, Y.; Ong, K. P.; Akimov, Y. A.; Wu, L.; Li, B.; Wu, J.; Huang, Y.; Liu, Q.; Png, C. E.; Gan, C. L.; Yang, P.; Zhang, H. Stabilization of 4H Hexagonal Phase in Gold Nanoribbons. *Nat. Commun.* **2015**, *6*, 7684.
(26) Fan, Z.; Zhang, H. Crystal Phase-Controlled Synthesis, Properties and Applications of Noble Metal Nanomaterials. *Chem. Soc. Rev.* **2016**, *45*, 63−82.
(27) Fan, Z.; Huang, X.; Chen, Y.; Huang, W.; Zhang, H. Facile Synthesis of Gold Nanomaterials with Unusual Crystal Structures. *Nat. Protoc.* **2017**, *12*, 2367−2378.
(28) Cheng, H.; Yang, N.; Lu, Q.; Zhang, Z.; Zhang, H. Syntheses and Properties of Metal Nanomaterials with Novel Crystal Phases. *Adv. Mater.* **2018**, *30*, 1707189.
(29) Liu, L.; Diaz, U.; Arenal, R.; Agostini, G.; Concepcion, P.; Corma, A. Generation of Pt Single Atoms and Clusters with Exceptional High Stability During Transformation of Two-Dimensional into Three-Dimensional Zeolite. *Nat. Mater.* **2017**, *16*, 132−138.
(30) Estebanez-Bloem, N.; Ferrera-Gonzalez, J.; Frances-Soriano, L.; Arenal, R.; Gonzalez-Bejar, M.; Perez-Prieto, J. Breaking the Nd^{3+}-Sensitized Up Conversion Nanoparticles Myth About the Need of Onion-Layered Structures. *Nanoscale* **2018**, *10*, 12297−12301.
(31) Roy, A.; Kundu, S.; Mueller, K.; Rosenauer, A.; Singh, S.; Pant, P.; Gururajan, M. P.; Kumar, P.; Weissmüller, J.; Singh, A. K.; Ravishankar, N. Wrinkling of Atomic Planes in Ultrathin Au Nanowires. *Nano Lett.* **2014**, *14*, 4859−4866.
(32) Zhu, Y.; He, J.; Shang, C.; Miao, X.; Huang, J.; Liu, Z.; Chen, H.; Han, Y. Chiral Gold Nanowires with Boerdijk−Coxeter−Bernal Structure. *J. Am. Chem. Soc.* **2014**, *136*, 12746−12752.
(33) Gao, M.; Zuo, J. M.; Twesten, R. D.; Petrov, I.; Nagahara, L. A.; Zhang, R. Structure Determination of Individual Single-Wall Carbon Nanotubes by Nanoarea Electron Diffraction. *Appl. Phys. Lett.* **2003**, *82*, 2703−2705.
(34) Arenal, R.; Kociak, M.; Loiseau, A.; Miller, D.-J. Determination of Chiral Indices of Individual Single- and Double-Walled Boron Nitride Nanotubes by Electron Diffraction. *Appl. Phys. Lett.* **2006**, *89*, 073104.
(35) You, H.; Liu, X.; Liu, H.; Fang, J. Theoretical Description of the Role of Amine Surfactant on the Anisotropic Growth of Gold Nanocrystals. *CrystEngComm* **2016**, *18*, 3934−3941.
(36) Halder, A.; Ravishankar, N. Ultrafine Single-Crystalline Gold Nanowire Arrays by Oriented Attachment. *Adv. Mater.* **2007**, *19*, 1854−1858.
(37) Feng, H.; Yang, Y.; You, Y.; Li, G.; Guo, J.; Yu, T.; Shen, Z.; Wu, T.; Xing, B. Simple and Rapid Synthesis of Ultrathin Gold Nanowires, Their Self-Assembly and Application in Surface-Enhanced Raman Scattering. *Chem. Commun.* **2009**, *0*, 1984−1986.
(38) Loubat, A.; Lacroix, L.-M.; Robert, A.; Impéror-Clerc, M.; Poteau, R.; Maron, L.; Arenal, R.; Pansu, B.; Viau, G. Ultrathin Gold Nanowires: Soft-Templating *versus* Liquid Phase Synthesis, a Quantitative Study. *J. Phys. Chem. C* **2015**, *119*, 4422−4430.
(39) Schmidbaur, H.; Schier, A. Aurophilic Interactions as a Subject of Current Research: an Up-Date. *Chem. Soc. Rev.* **2012**, *41*, 370−412.
(40) Koizumi, H.; Oshima, Y.; Kondo, Y.; Takayanagi, K. Quantitative High-Resolution Microscopy on a Suspended Chain of Gold Atoms. *Ultramicroscopy* **2001**, *88*, 17−24.
(41) Legoas, S. B.; Galvão, D. S.; Rodrigues, V.; Ugarte, D. Origin of Anomalously Long Interatomic Distances in Suspended Gold Chains. *Phys. Rev. Lett.* **2002**, *88*, 076105.
(42) Mackay, A. L. A. Dense Non-Crystalloraphic Packing of Equal Spheres. *Acta Crystallogr.* **1962**, *15*, 916−918.
(43) Onsager, L. *Ann. N. Y. Acad. Sci.* **1949**, *51*, 627−659.
(44) Mohr, F.; Jennings, C.; Puddephatt, R. J. Self-Assembly in Gold(I) Chemistry: A Double-Stranded Polymer with Inter-strand Aurophilic Interactions. *Angew. Chem., Int. Ed.* **2004**, *43*, 969−969.
(45) Leelavathi, A.; Madras, G.; Ravishankar, N. Ultrathin Au Nanowires Supported on rGO/TiO_2 as an Efficient Photoelectrocatalyst. *J. Mater. Chem. A* **2015**, *3*, 17459−17468.
(46) Calle-Vallejo, F.; Loffreda, D.; Koper, M. T.; Sautet, P. Introducing structural sensitivity into adsorption−energy scaling relations by means of coordination numbers. *Nat. Chem.* **2015**, *7*, 403−410.
(47) Hajiw, S.; Pansu, B.; Sadoc, J.-F. Evidence for a C14 Frank−Kasper Phase in One-Size Gold Nanoparticle Superlattices. *ACS Nano* **2015**, *9*, 8116−8121.
(48) Lee, S.; Leighton, C.; Bates, F. S. Sphericity and Symmetry Breaking in the Formation of Frank−Kasper Phases from One Component Materials. *Proc. Natl. Acad. Sci. U. S. A.* **2014**, *111*, 17723−17731.
(49) Hobbs, D.; Hafner, J.; Spišák, D. Understanding the Complex Metallic Element Mn. I. Crystalline and Noncollinear Magnetic

DOI: 10.1021/acsnano.8b05036
ACS Nano 2018, 12, 9521−9531

Structure of α-Mn. *Phys. Rev. B: Condens. Matter Mater. Phys.* **2003**, *68*, 014407.
(50) Petkov, V. Nanostructure by High-Energy X-ray Diffraction. *Mater. Today* **2008**, *11*, 28−38.
(51) McGreevy, R. L.; Pusztai, L. Reverse Monte Carlo Simulation: A New Technique for the Determination of Disordered Structures. *Mol. Simul.* **1988**, *1*, 359−367.
(52) Kresse, G.; Furthmüller, J. Efficient Iterative Schemes for *Ab Initio* Total-Energy Calculations Using a Plane-Wave Basis Set. *Phys. Rev. B: Condens. Matter Mater. Phys.* **1996**, *54*, 11169−11186.

DOI: 10.1021/acsnano.8b05036
ACS Nano 2018, 12, 9521−9531